3D Flexible and Robust HAPs/PVA Separator Prepared by Freezing-Drying Method for Safe Lithium Metal Batteries

Wei Wang[†,‡], *Can Liao*[†], *Kim Meow Liew*[‡], *Zonghai Chen*[§], *Lei Song*[†], *Yongchun Kan*[†,*], *and Yuan Hu*[†,*]

[†] State Key Laboratory of Fire Science, University of Science and Technology of China, 96 Jinzhai Road, Hefei, Anhui 230026, People's Republic of China

[‡] Department of Architecture and Civil Engineering, City University of Hong Kong, Tat Chee Avenue, Kowloon, Hong Kong

[§] Chemical Sciences and Engineering Division, Argonne National Laboratory, Argonne, IL 60439, USA

E-mail: yuanhu@ustc.edu.cn (Y. Hu); yckan@ustc.edu.cn (Y. C. Kan)

Keywords: Separator; Polyvinyl alcohol; Hydroxyapatite; Safety; Li metal batteries.

Abstract: Lithium (Li) metal batteries have shown great promise for next-generation electrical energy storage due to unique features of lithium metal like light weight and high specific capacity all anode materials. Nevertheless, the uncontrollable growth of dendritic and mossy Li, resulting in a low Coulombic efficiency and serious safety concerns, has hindered the practical application of rechargeable Li-metal batteries. Here we report an environmentally friendly nanocomposites separator, comprising of polyvinyl alcohol and hydroxyapatite, which exhibits outstanding Young's modulus and high mechanical flexibility. We show that this separator can efficiently suppress the growth of dendritic Li and enable a homogeneous stable solid electrolyte interphase. Compared to lithium metal batteries using a commercial polyolefin-based separator, cells using the reported nanocomposite separator

demonstrate a superior electrochemical performance with a much higher Coulombic efficiency during the charge/discharge cycling at a practical current density of 2 mA cm^{-2}. This work indicates that nanocomposite engineering could be a promising strategy to develop stable, safe and sustainable Li-metal batteries.

1. Introduction

Lithium ion rechargeable batteries have achieved great successes during the past three decades since their commercialization in 1991 using graphite to replace Li metal as the anode. Nevertheless, their limited energy density still cannot meet the ever-growing requirement for applications such as electrical vehicles, grid-scale stationary storage systems, auto-aircraft, etc. In this regard, extensive effort has been dedicated to developing alternative anodes with a higher capacity, for instance, silicon, tin and Li metal.[1-5] Among all, fabricating lithium metal batteries by replacing graphite with lithium metal as the anode is generally recognized as an effective way to dramatically enhance the energy density. Li metal is an ideal anode material for lithium based rechargeable batteries owing to its highest theoretical specific capacity (3860 mAh g^{-1}), the lowest anode potential (-3.04 V vs standard hydrogen electrode) and low gravimetric density (0.53 g cm^{-3}).[6, 7] Therefore, it is considered as the "holy Grail" of battery chemistry. Moreover, Li metal is also adopted as the working anode for several promising beyond lithium-ion technologies such as lithium/sulfur batteries and lithium/oxygen batteries.[8-12] However, uncontrollable Li dendrite growth together with a low coulombic efficiency during charge/discharge process have severely impeded the further development of rechargeable Li metal batteries.[13-15] To our knowledge, highly reactive Li metal could spontaneously react with organic electrolytes and Li salt to constantly generate the solid electrolyte interphase (SEI) layer, which is characterized by ionic conduction but electron insulation. Although the formation of SEI layer can prevent the further reaction between electrolyte and Li metal, it cannot endure the mechanical deformation during Li deposition/stripping process and thus results in the generation of surface defects on SEI layer.[16-18] Subsequently, dendritic and mossy Li tend to germinate at these surface defects where the current density is locally concentrated, and meanwhile the new SEI layers are also formed during this process. As a consequence, the reduplicative breakage and repair of SEI layer lead to the constant consumption of electrolytes and growth of "dead Li", thus resulting in the low coulombic efficiency and capacity fading.[19-21] Moreover, after repeated uneven Li deposition/stripping process, Li dendrites can eventually pierce through the separators and lead to internal short circuits and sometimes catastrophic failure. Hence, to meet the ever-increasing demand of batteries with high energy density, developing stable and safe Li metal batteries has always been pivotal and remains an ongoing challenge.

To date, plenty of efforts have been devoted to revealing the detailed mechanism of the Li dendrite formation. Chazalviel proposed that the large electric field caused by the anion depletion near cathode could lead to the growth of Li dendrites.[22] This theory indicates that electrolytes with high ionic conductivity and stable anion mobility are beneficial for preventing anion depletion, and thus to some extent relieving the generation of Li dendrites. On the other hand, it is recognized that as the Young's modulus of separator is twice that of Li metal, the interfacial roughening could be mechanically suppressed.[23] According to the abovementioned two strategies, many approaches have been proposed to build Li metal batteries with suppressed Li dendrites formation, for instance, using suitable electrolyte additives,[24, 25] solid phase electrolytes,[26-28] network polymer electrolytes,[29] organic or/and inorganic-coated separators,[30, 31] three-dimensional current collector.[32-34] In recent years, constructing mechanical protective layers is of particular interests to impede the growth of Li dendrites and to achieve satisfactory coulombic efficiency. Cui fabricated a monolayer of interconnected amorphous hollow carbon nanospheres on Li metal anode to isolate the Li metal deposition and facilitate the formation of stable SEI layer.[35] By the way, Cui also prepared a trilayer separator with a structure of polyethylene/SiO_2 particles/ polyethylene to delay the penetration of Li dendrites through the separator, and thus prolonging the life of batteries.[36] Hu architected a thermally conductive separator, mainly comprising of boron-nitride nanosheets, to improve the electrochemical stability of Li metal anodes.[37] Additionally, Guo et al. designed an artificial Li_3PO_4 SEI layer to restrain the unfavorable reaction between the Li metal and the electrolyte and the dendritic Li growth in $LiFePO_4$|Li systems.[17] Nevertheless, in most cases, complicated process (such as synthesis of templates or artificial SEI layer, complex manufacturing process), expensive instrumentation requirements, high cost of time consuming and raw materials restrain the further practical application. Moreover, even with numerous efforts, the long-time suppression of dendritic Li growth in high current density (>0.5 mA cm^{-2}) is still a challenging task impeding Li metal batteries to be materialized in market.

Inspired by the aforementioned works, herein we designed a new class of eco-friendly separator consisted of degradable polyvinyl alcohol (PVA) and hydroxyapatite nanorods (HAPs) by using a feasible Freeze-drying method. The corresponding preparation routes are depicted in Figure S1 (Supporting Information). To our knowledge, PVA resin without cross-linking structures also exhibits high mechanical strength due to its internal hydrogen bonds, which, however, are unbeneficial for the formation of three-dimensional porous structures required by separators. By using the Freeze-drying method, the hydrogen bonds are significantly suppressed, and separators with high porosity can be obtained. On one hand, HAPs, as a biomaterial and the main component of bones, can provide much needed mechanical strength and the consequently formed three dimensional (3D) networks within PVA are anticipated to inhibit the Li Dendrites growth in Li metal batteries and thereby enhance the safety as well as extending the battery life. On the other hand, HAPs with one-dimensional disorder structures in PVA porous networks could greatly improve the porosity and compatibility with electrolytes. The crystalline structure, morphologies and thermal stability are discussed in Supporting Information (Figure S2). Herein, it should be noted that at least four properties could make the 3 D HAPs/PVA separator advanced and efficient: (1)

Due to the excellent mechanical properties of PVA, HAPs/PVA separator exhibits a high flexibility and satisfying tensile strength, which are of great importance for further application. Besides, HAPs/PVA separators are capable of highly thermal stability superior than polyolefin-based separators, making it possible for high-temperature application. (2) In the case of the HAPs,[38-40] it will provide much high Young's modulus enough to prevent the penetration of Li dendrites. Even if HAPs are partially embedded underneath PVA matrix, the growth trend of dendritic Li may still be suppressed by HAPs after piercing through the surface PVA layer. Moreover, the 3D network structure architected by HAP one dimensional rods can fully prevent the further growth in large area in the direction towards separators. Then, Li dendrites will grow more in a direction perpendicular to the separator and thereby limit each other's growth space, which represent a lower surface area, avoiding the unnecessary consumption of electrolyte and Li metal, and thus achieving a higher Coulombic efficiency. (3) In this work, Freeze-drying method is first proposed to fabricate PVA separator by successfully suppressing the hydrogen bonds reaction within the structures of PVA itself and achieve a high porosity. Incorporating with 3D HAPs network will improve the thermal behavior of separator as well as further optimize the porosity of PVA porous separator, which can facilitate the transport of Li ions and outstanding wettability with electrolytes. Moreover, PVA and HAPs are rich in polar functional groups and thus possess a better affinity with polar electrolytes. Hence, such an advanced membrane combining the function of suppressing dentritic Li and the properties of separator itself is unprecedented and rarely reported. (4) To our knowledge, PVA is a nontoxic and bio-degradable polymer and extremely safe and healthy for human. HAPs as well as PVA all have good biocompatibility and exhibit environmentally friendly, which can meet the requirement of environment protection and be friendly to the health of nature. Moreover, PVA and HAPs are commercially cheap, the preparation procedure of PVA/HAPs membrane are quite simple and controllable. These advantages make it possible for the separator to be further applied in industrial field.

2. Results and discussion

Owing to strong substantial interaction by hydrogen bonds, it is of great difficulty to build a PVA membrane with high porosity at regular temperature. As a control experiment, we immerse a membrane of PVA and HAPs (HAPs10%PVA) in an ethanol bath. After fully soaked with the ethanol, the membrane was dried at the room temperature (25 ^{o}C) by naturally evaporating the absorbed ethanol. After drying, the membrane exhibits no obvious porous structure (Figure S3, Supporting Information), which illustrates that it is failure to build porous membrane under the regular temperature. Alternatively, a Freeze-drying method was utilized to build a porous framework of PVA/HAPs composites by reducing the reconfiguration of polymer chains during the removal of solvent (ethanol) at a reduced temperature. The scanning electron microscopy (SEM) images of the as-prepared PVA and PVA/HAP separators fabricated under Freeze-drying method are shown in Figure S4b-f, Supporting Information. Through the observation of cross-section, the hierarchical maze-like porous three-dimensional structure are formed after using the Freeze-drying method. The enlarged porous structure can greatly benefit for enhancement of the wettability with electrolytes and improve the ion diffusion efficiency. In the case of HAPs-filled PVA membranes, SEM images exhibit that after the incorporation of HAPs, the holes covered on the surface are enlarged and more intricate. Simultaneously, as the loading of HAPs increases up to 10 % and 20 %, the porous structures are further grown but by the appearance of agglomeration morphology (Figure S4e and f, Supporting Information), which may prejudice to their mechanical properties. For the purpose of a fair comparison, SEM images of commercial polyolefin-based separator are presented in Figure S4a (Supporting Information). It can be obviously observed that the porous structures are much smaller than that of PVA-based separators synthesized by the Freeze-drying method, which are unbeneficial for the affinity with electrolytes and Li-ion diffusion efficiency. In addition, the porosity data in detail is depicted in Figure S5 (Supporting Information). By the way, results also demonstrate that the enlarged porosity (>70%) of HAPs/PVA separators could effectively enhance the compatibility with polar liquid electrolytes achieving high electrolyte uptake and lower contact angles (Discussed in Figure S6-9, Supporting Information).

Actually, separators with high mechanical properties and great flexibility are extremely important for both the wide application and safety of batteries. Excellent mechanical performance should not only be robust enough to withstand the high tension upon assembling and casual collision, but also prevent internal short circuits induced from dendrite growth. Generally, it is recognized that inorganic mineral-filled nanocomposites may show a worse mechanical behavior. In this work, to have a more intuitive view of the as-prepared HAPs/PVA separators, the sample of HAPs20%/PVA membrane is chosen for display. The photos in **Figure 1**a, b exhibit the flexibility of HAPs20%/PVA under different bending condition including rolled and twisted. Furthermore, the separator could be rolled at least 10 time with a relative low value of radius (< 0.5 mm) (Figure 1c). After keeping the rolled state for 30 min, HAPs20%/PVA separator is restored to its original state without any visible damages (Figure 1d), indicating the great mechanical strength and high flexibility of this novel class of HAPs/PVA separator.

Well dispersion of HAPs in PVA substrate is very important for the construction of porous architecture and mechanical performance. SEM image of HAPs10%/PVA separator (a relative high loading selected as representative one) shown in Figure 1e exhibits a homogeneous maze-like structure with high porosity, indicating a successful fabrication procedure. Element mapping technique is employed to intrinsically observe the distribution of HAPs. Figure 1f shows the morphology of the sample. The uniform element pots of calcium and phosphorus respectively depicted in Figure 1g and Figure 1h strongly prove its excellent dispersion state, which indicates that during the fabrication procedure, there exists no obvious precipitation phenomenon from inorganic nanorods even at a high loading of 10 wt.%. This interesting results could be explained by the strong substantial interfacial interaction caused by hydrogen bonds and Van der Waals force.

Nowadays, a high efficiency separator with green, eco-friendly and easy-handling features is necessary and urgent. To further intuitively present the feature of HAPs10%/PVA separators, the separator with a shape of circle (16 mm) (Figure 1k) is dipped in deionized water and immediately filled with water, indicating a high affinity with water (Figure 1l). After 20 s of shaking, this separator has been completely shattered to pieces with a mainly partial dissolved in deionized water. Indeed, PVA and HAPs are all environmentally friendly and completely nontoxic to humans. Therefore, the as-prepared PVA/HAPs separator can meet the requirement of any environmental and health policy.

One serious safety issue of polyolefin-based separators is their thermal shrinkage concerns. In most cases, highly thermal stability of separators means a safer LIBs running at high temperature, especially for the large-scale and/or high-power and energy devices. The thermal shrinkage photos and the corresponding statistics of Celgard separator, control PVA and HAPs/PVA separators after with thermal treatment at 100, 120, 140, 160, and 180 ℃ for 0.5 h were concluded in Figure S11-12 (Supporting Information). After thermal treatment at 120 ℃ for 0.5 h, Celgard separator shows a sharp decrease of surface area. Oppositely, PVA-based separators can maintain the original shape under the same condition, revealing a great thermal stability. To further investigate the thermal stability of the as-prepared separators, differential scanning calorimeter (DSC) technique is conducted. As is shown in Figure S13, Celgard separator exhibits a broad endothermic peak from 150 ℃ to 180 ℃, which attributes to the softening and melting of polyolefin, but PVA and HAPs/PVA shows no obvious endothermic peak below 200 ℃, indicating that PVA-based separator can hold a better thermal stability compared with Celgard separator. Herein a micro-combustion calorimeter (MCC) measurement was carried out to approximately study the heat release of separators under high temperature, which can similarly evaluate the safety index when fire accident happens. The key parameters including peak heat release rate (PHRR) and total heat release (THR) are depicted in Figure S14. Celgard separator exhibits a PHRR value of 1300 W g^{-1} much higher than PVA (314 W g^{-1}) and HAPs10%/PVA (173 W g^{-1}). HAPs10%/PVA separator also achieves a lower THR value (23 kJ g^{-1}) than Celgard separator (42 kJ g^{-1}) and PVA separator (33 kJ g^{-1}). Therefore, HAPs/PVA separators with an excellent flame retardancy and thermal shrinkage behavior are expected to impart LIBs with high safety when a fire issue occurs.

The stress-strain behavior of Celgard, PVA and HAPs/PVA separators has also been studied, the corresponding results are presented in Figure 1i and j. In fact, owing to the uniaxial stretching fabrication process, the tensile strength of Celgard separator is determined by the orientation. Celgard separator possesses a tensile strength of 90.5 MPa along the machine direction and 14.2 MPa along the transversal direction. In the case of PVA separator, the tensile strength is about 17.1 MPa, which exhibits excellent mechanical performance. After hybridizing with 1 wt. % of HAPs, the tensile strength of HAPs/PVA separators is greatly increased to 23.2 MPa, attributing to the synergistic combination of hydrogen bonding and van der Waals force. With the increase of the loading of HAPs, the tensile strength shows a decreasing trend, but also superior to Celgard separators until up to the loading of 20 wt.%. From a macro perspective, the HAPs/PVA separator exhibits a considerably higher Young's modulus (833 MPa, 652 MPa and 630 MPa with a HAPs loading of 20 wt.%, 10 wt.% and 1 wt.%, respectively) compared with the Celgard separator (143 MPa) and PVA separator (278 MPa). Usually, the high Young's modulus of separators is advantageous for holding structural integrity and hindering the rupture if an accidental crash occurs. Besides, the higher Young's modulus and mechanical strength of PVA/HAPs can also exhibit a considerable promising potential to retard the growth of lithium dendrite, thereby improving the safety of batteries. Moreover, the as-prepared HAPs/PVA separators with higher mechanical performance and Young's modulus over the commercial Celgard separator at the transversal direction could be robust enough for battery fabrication procedure.

Different from the Young's modulus evaluated by tensile strength, the surface Young's modulus of separator from a micro view can determine whether the tough surface can effectively suppress the dendritic Li growth or not. As proposed by Newman and Balsara, a solid layer with a Young's modulus higher than 6 GPa could sufficiently retard the growth of Li dendrites.[23, 41] In order to further investigate the surface Young's modulus of separators, the atomic force microscopy (AFM) using a tapping mode was deployed. It can be clearly observed that HAPs10%/PVA separator achieves a much higher Young's modulus (**Figure 2**f) than Celgard separator (Figure 2d) and pristine PVA separator (Figure 2e). The partial modulus in detail (Figure S15, Supporting Information) indicate that HAPs10%/PVA can present an average Young's modulus of near 40 GPa (Figure S15d, Supporting Information) higher than those of Celgard and pure PVA separators (both ~/< 1 GPa). Unlike the structure of pristine PVA separator (Figure 2a), after incorporating HAPs, a 3D network consisting of HAPs is formed inside the PVA matrix (Figure 2b). The desired 3D HAPs network is anticipated to sufficiently retard the growth of Li dendrites. Here it should be noted that: 1) Because of the coverage of PVA matrix, HAPs10%/PVA exhibits an uneven Young's modulus mapping described in Figure 2c; 2) The AFM probe used here has a detecting region of about 500 MPa to 50 GPa, the region in Figure 2f showing a modulus higher than 100 GPa has a limited reference value. Moreover, it is also worth noting that the tensile strength and Young's modulus of the as-prepared HAPs10%/PVA separator shows higher values than those for previously reported inorganic separators (Table S1, Supporting Information).

To investigate the electrochemical performance, the as-prepared separators are conducted in Cu|Li cells, where Cu foil is employed as the working electrode, Li foil used as the counter/reference electrode, and 1 M $LiPF_6$ in ethylene carbonate/diethyl carbonate (1: 1 by volume) without any additive as the electrolyte. The Li dripping/stripping process between the working electrode and the counter/reference electrodes are conducted at the current densities of 0.5 mA cm^{-2}, 1 mA cm^{-2} and 2 mA cm^{-2}, matching the requirement of practical applications.

The areal capacity for each Li deposition was set to be 1 mAh cm^{-2}. Coulombic efficiency, an important parameter to examine for a practical Li metal anode, is calculated as the ratio of the amount of Li stripped from Cu working electrode versus the deposited amount. **Figure 3**a shows the potential profile in the third cycle for the cells using Celgard separator and HAPs10%/PVA separator. It is clear that there exists a similar overpotential at the initial Li deposition process for both cells, revealing that HAPs10%/PVA separator does not result in a higher impedance, which is also proven by electrochemical impedance spectroscopy measurement (Figure S10). However, after repeating dripping/stripping process for near 70 cycles, the cell using Celgard separator exhibits an unstable profile, while HAPs10%/PVA separator cell still shows a stable stripping process after 100 cycles (Figure 3c) with a Coulombic efficiency of near 91% (Figure 3b). When the current density is increased to 1 mA cm^{-2} even 2 mA cm^{-2}, the cells employing HAPs10%/PVA separator still maintain a more stable coulombic efficiency and longer cycles (Figure 3f and i), near 89% and 87% for more than 100 cycles at 1 mA cm^{-2} and 2 mA cm^{-2} respectively. In comparison, the Celgard separator cell shows a quick decay in Coulombic efficiency and unstable cycling behavior. After about 24 cycles, the Coulombic efficiency decreases to less than 50% at 2 mA cm^{-2} (Figure 3h). The poor Coulombic efficiency stability of the cell using Celgard separator is due to the continuously formation of dendritic and mossy Li, which constantly consumes the electrolytes and Li ions, causing the growth of the SEI layer. It should be noted that the average Coulombic efficiency of the cells with HAPs10%/PVA achieves near 89% for 100 cycles in this work, while Li metal cycling in normal carbonate electrolyte only maintains a Coulombic efficiency of about 85%.[42] Moreover, when we compare the voltage hysteresis of the two separators, it can be clearly found that HAPs10%/PVA separator always has a smaller voltage hysteresis than the Celgard separator. It can be ascribed to the lower interfacial resistance, illustrating a much more stable SEI layer formed underneath HAPs/PVA separator.

Actually, HAPs/PVA separator with a relative low HAPs loading cannot form a dense 3D HAPs network to efficiently suppress the growth of Li dendrites. Among as-prepared separators, only when the loading of HAPs is up to 10 wt.%, HAPs/PVA separator can achieve a good Coulombic efficiency. We also conducted the cells using pristine PVA separator, HAPs5%/PVA and HAPs20%/PVA (Figure S16, Supporting Information). The cells using pristine PVA separator and HAPs5%/PVA separator show unstable cycling process. Especially in the case of pristine PVA separator, it does not maintain a stable behavior even during initial cycles; we ascribe this to the high porosity of PVA separator. Although high porosity endow control PVA separator with outstanding electrolyte uptake and better wettability, it cannot prevent the constantly growth of Li dendrites due to the low Young's modulus. On the contrary, the high porosity can easily make the Li dendrites pierce through the empty space and lead to the constantly repeated the construction/repair SEI layer process. Likewise, the low loading of HAPs cannot fabricate a well 3D HAPs network and effectively suppress the growth of Li dendrites. The results demonstrate that only when the addition of HAPs reaches 10 wt.%, a well dense 3D HAPs network can be architected as schematically shown in Figure 2b. Herein, we declare that the HAPs/PVA separators with loading over 10 wt.% can be regarded as the 3D HAPs/PVA separator. And, the separator of HAPs10%/PVA separator will be renamed as 3D HAPs/PVA separator and chosen as a representative sample for following evaluation and comparison to the Celgard separator.

Figure 4a-c schematically illustrate the morphological difference of Li deposited on the copper substrate with the Celgard separator and 3D HAPs/PVA separator. In the case of the cell using the Celgard separator, the polyolefin-based separator with a low modulus does not prevent the continuously growth of dendritic Li. For this reason, there exists a repeated construction/repair process for SEI layer, which leads to the constant consuming of electrolyte and Li ion and an inhomogenous SEI layer, consequently causing the low Coulombic efficiency and short circuit. In comparison, because of the high modulus, 3D HAPs/PVA separator can efficiently retard the growth of Li dendrites vertically perpendicular to the separator. Different from the dendritic Li formed underneath Celgard separator, the Li deposition by the constraint of 3D HAPs/PVA separator presents a smaller SEI layer specific surface area and nondendritic-like Li, which consuming less electrolytes and Li-ion. As the cycling process continues, the SEI layer tends to become smooth and achieve a stable and uniform surface, which could efficiently suppress the growth of dendritic Li. The corresponding experimental results are presented in Figure 4d-m. SEM images shows that after the first deposition of a fixed amount of Li on the planar surface of copper substrate (Figure 4d, i) with the Celgard separator, the surface of substrate are full of dendritic and mossy Li (Figure 4e, j), confirming that Celgard separator cannot change the ramified growth of the dendrites. Moreover, after 40 cycles of galvanostatic stripping/plating process, rough surface and excessive dendritic and mossy Li growth can be clearly observed (Figure 4f, k). In comparison, for the 3D HAPs/PVA separator, after the first deposition of the same amount of Li on the copper surface, it can be found the scale of dendritic Li are larger than that with Celgard separator, and the surface are comparably smoother and more uniform than that with Celgard separator (Figure 4g, l). A Li deposition modelling proposed by Tang revealed that for planar electrodes, the Li deposition process occurs preferentially at the edge of electrode due to the higher concentration of Li-ion flux at the edge region than that at the centre part.[43] The digital photos provided in Figure S17a (Supporting Infromation) show that the Li deposition with Celgard separator exhibits an uneven surface on bare copper substrate, the deposited Li at the edge of electrodes shows a much rougher morphology than that in the centre region. However, for the 3D HAPs/PVA separator, with a same amount of Li deposition, there exhibits a uniform and smooth surface in the whole area (Figure S17b, Supporting Information), which is probably due to the high ion-conductivity and uniform Li-ion concentration distribution. Interestingly, after dripping/stripping process for 100 cycles, the surface becomes smoother; no excessive dendrites formation can be found, revealing a well-confined Li cycling behavior caused by the 3D HAPs/PVA separator. Such drastically different morphologies further confirm the superior advances of the 3D HAPs/PVA separator on Li dendrites suppression.

The electrochemical stabilities of the as-prepared PVA-based separators within the operation voltage of a battery are investigated by the linear sweep voltammetry. The results presented in Figure S18 (Supporting Infromation) revealed that PVA-based separators with the carbonate electrolytes exhibit no obvious decomposition around 5.0 V vs Li^+/Li, which even represents a higher electrochemical stability than Celgard separator, which is favorable for their electrochemical properties. To verify the potential of the as-prepared separators for LMBs, $LiFePO_4$|Li cells with the Celgard and PVA-based separators are assembled. The electrochemical properties of the cells are conducted at a cycling rate of C/5 (1C = 170 mA g^{-1}) and a cutoff voltage of 2.8-4.2 V. As shown in **Figure 5**a, among the cells with the different separators, 3D HAPs/PVA separator illustrates the best cycling stability, showing a high capacity retention of about 97.3% after 100 cycles and a steadily Coulombic efficiency (~ 100%), whereas, PVA separator with carbonate electrolytes exhibits a relative low capacity retention (~ 90%) and Coulombic efficiency (~ 96%) even worse than those of Celgard separator with a capacity retention (~ 90%) and Coulombic efficiency (~ 99%), which is probably due to the poor ion conductivity and continuously generation and growth of new SEI layer. Moreover, Figures S19a,b (Supporting Information) also present the specific discharge capacity and the Coulombic efficiency of the cells using the HAPs-based separators with different loadings. The specific discharge capacity of the cell with HAPs-based separators all exhibit a higher capacity retention than the cells using Celgard and pristine PVA separators. Furthermore, the voltage curves confirm that the cell using the 3D HAPs/PVA, after 100 cycles, has a more stable charging and discharging voltage platform with a smaller voltage gaps and a capacity retention of 146.6 mAh g^{-1} (Figure S20c, Supporting Information), superior to the cells using the Celgard separator (Figure S20a, Supporting Information) and pristine PVA separator (Figure S20b, Supporting Information). Based on the above results, it can be illustrated that the 3D HAPs networks can enable the cell of a stable cycling performance and meanwhile eliminate the disadvantage of relative low coulomb efficiency of the control PVA separator.

The rate capability always indicates the potential of batteries, which are of extremely importance in the field of EV, HEV and large-scale energy-storage applications. The rate capability of the cells using various separators are presented in Figure 5b. As displayed, the PVA separator based cell exhibits a comparable specific capacity to the cell with Celgard separator at low C-rate (< C/2), but worse at high C-rate. In contrast, the cell using 3D HAPs/PVA separator exhibits a desired C-rate capability, achieving a discharge capacity of over 130 mAh g^{-1} at a C-rate of 2C (Figure 5e), much better than the those of the cells using the Celgard separator (110 mAh g^{-1}) (Figure 5c) and pristine PVA separator (90 mAh g^{-1}) (Figure 5d). When zooming in, we can find that the cell using 3D HAPs/PVA separator exhibits smaller voltage gaps at all various current density (Figure S21c, Supporting Information) compared with the cells using the Celgard separator (Figure S21a, Supporting Information) and the control PVA separator (Figure S21b, Supporting Information), indicating a decreased polarization. To further investigate the dynamical stability of Li/electrolyte soaked 3D HAPs/PVA separator, we fabricate the Li|electrolyte soaked separator|Li symmetric cells, which are charged and discharged for respective 3 h during each cycle, employing a constant current density of 0.5 mA cm^{-2} (Figure 5f). In the case of the cell with Celgard separator, at the beginning cycling stage, the overpotential for dripping/stripping of Li metal is near 40 mV and meanwhile increases rapidly. For the pristine PVA separator, the cell also exhibits a high voltage polarization in the first 30 cycles for the electrode activation and continuously formation of the new SEI layer. In comparison, the cell using 3D HAPs/PVA separator has a good cycling stability under the same condition. Except for the relatively high voltage polarization at the first five cycles for formation of stable SEI layer, the cell achieves an extremely low overpotential of 4.2 mV for over 600 h without short circuit, revealing that growth of dendritic Li can be effectively suppressed and thus promotes a stable SEI layer. Therefore, it can be demonstrated that such an excellent compatibility between 3D HAPs/PVA separator and the Li metal electrode enables a long cycling life for the produced batteries.

To further investigate the potential of 3D HAPs/PVA separator in high-temperature application, we conducted the $LiFePO_4$|Li batteries using the lithium bis(oxolato)borate/propylene carbonate electrolytes system operated at 110 ℃ (Figure S22b, Supporting Information). In fact, conventional polar carbonate electrolytes have poor compatibility with non-polar commercial polyolefin separators, which leads to a poor electrochemical performance (Figure S22a, Supporting Information). In comparison, the 3D HAPs/PVA separator exhibits a high affinity with polar electrolytes due to its plenty of polar hydroxyl groups and thus results a high cycling capacity of 147 mAh g^{-1} and a retention of ~ 100% for over 50 cycles at a rate of 0.5 C. Under the high temperature (110 ℃), the $LiFePO_4$|Li cell with 3D HAPs/PVA separator exhibits a stable discharge capacity in the first 10 cycles, and consequently has a downward trend. The results discussed in front illustrate that 3D HAPs/PVA separator exhibits the potential for relative high-temperature Li metal batteries.

3. Conclusion

In summary, a feasible, environmentally friendly and cost-effective strategy has been introduced to prepare a highly flexible 3D HAPs/PVA separator, which presents an unprecedented combination of mechanical properties, thermal stability, ion-conductivity. Importantly, due to high Young's modulus induced by the 3D HAPs network, this unique 3D HAPs/PVA separator can allow the Li metal anode steadily cycling up to a practical current density of 2 mA cm^{-2} with an areal capacity of 1mAh cm^{-2}. The Coulombic efficiency shows stable at 87% for over 100 cycles, illustrating the effectively suppressed growth of dendritic

Li and formation of the stable and homogenous SEI layer. Moreover, the 3D HAPs/PVA separator employed in $LiFePO_4$|Li metal batteries also illustrated that this novel separator can enable LMBs of better electrochemical performance and lower polarization compared to cells based on the Celgard separator. We believe that this interesting separator capable of feasible synthesis process and various desirable advantages maybe offer a promising separator candidate for the next-generation high-energy-density rechargeable battery systems such as lithium-sulfur and lithium-oxygen batteries, as well as other metal-based batteries.

Acknowledgements

This work was supported by National Natural Science Foundation of China (51704269); Fundamental Research Funds for the Central Universities (WK2320000037); National Basic Research Program of China (973 Program) (2014CB931804); the Research Grants Council of the Hong Kong Special Administrative Region, China (Project number 9042476 CityU 11201817); and National Natural Science Foundation of China (51573173).

Supporting Information

Supplementary figures, table and texts. (PDF)

References

1. L. Zhang, X. Hu, C. Chen, H. Guo, X. Liu, G. Xu, H. Zhong, S. Cheng, P. Wu and J. Meng, *Adv. Mater.*, 2017, **29**, 1604708.
2. X. Fan, T. Gao, C. Luo, F. Wang, J. Hu and C. Wang, *Nano energy*, 2017, **38**, 350-357.
3. H. Shang, Z. Zuo, L. Yu, F. Wang, F. He and Y. Li, *Advanced Materials*, 2018, 1801459.
4. J. Qian, W. A. Henderson, W. Xu, P. Bhattacharya, M. Engelhard, O. Borodin and J.-G. Zhang, *Nat. Commun.*, 2015, **6**, 6362.
5. D. Lin, Y. Liu and Y. Cui, *Nat. Nanotechnol.*, 2017, **12**, 194.

6. J.-M. Tarascon and M. Armand, in *Materials For Sustainable Energy: A Collection of Peer-Reviewed Research and Review Articles from Nature Publishing Group*, World Scientific, 2011, pp. 171-179.

7. W. Xu, J. Wang, F. Ding, X. Chen, E. Nasybulin, Y. Zhang and J.-G. Zhang, *Energ. Environ. Sci.*, 2014, **7**, 513-537.

8. Q. Pang, X. Liang, C. Y. Kwok and L. F. Nazar, *Nat. Energy*, 2016, **1**, 16132.

9. R. Fang, S. Zhao, Z. Sun, D. W. Wang, H. M. Cheng and F. Li, *Adv. Mater.*, 2017, **29**, 1606823.

10. B. Zhou, L. Guo, Y. Zhang, J. Wang, L. Ma, W. H. Zhang, Z. Fu and Z. Peng, *Adv. Mater.*, 2017, **29**, 1701568.

11. X. Zhang, Q. Zhang, X.-G. Wang, C. Wang, Y.-N. Chen, Z. Xie and Z. Zhou, *Angew. Chem.*, 2018.

12. D. Lei, K. Shi, H. Ye, Z. Wan, Y. Wang, L. Shen, B. Li, Q. H. Yang, F. Kang and Y. B. He, *Adv. Funct. Mater.*, 2018, 1707570.

13. W. Li, H. Yao, K. Yan, G. Zheng, Z. Liang, Y.-M. Chiang and Y. Cui, *Nat. Commun.*, 2015, **6**, 7436.

14. M. H. Ryou, D. J. Lee, J. N. Lee, Y. M. Lee, J. K. Park and J. W. Choi, *Adv. Energy Mater.*, 2012, **2**, 645-650.

15. G. Li, Y. Gao, X. He, Q. Huang, S. Chen, S. H. Kim and D. Wang, *Nat. Commun.*, 2017, **8**, 850.

16. S.-O. Tung, S. Ho, M. Yang, R. Zhang and N. A. Kotov, *Nat. Commun.*, 2015, **6**, 6152.

17. N. W. Li, Y. X. Yin, C. P. Yang and Y. G. Guo, *Adv. Mater.*, 2016, **28**, 1853-1858.

18. Y. Liu, D. Lin, P. Y. Yuen, K. Liu, J. Xie, R. H. Dauskardt and Y. Cui, *Adv. Mater.*, 2017, **29**, 1605531.

19. X. B. Cheng, T. Z. Hou, R. Zhang, H. J. Peng, C. Z. Zhao, J. Q. Huang and Q. Zhang, *Adv. Mater.*, 2016, **28**, 2888-2895.

20. Q. Yun, Y. B. He, W. Lv, Y. Zhao, B. Li, F. Kang and Q. H. Yang, *Adv. Mater.*, 2016, **28**, 6932-6939.

21. R. Zhang, N. W. Li, X. B. Cheng, Y. X. Yin, Q. Zhang and Y. G. Guo, *Adv. Sci.*, 2017, **4**, 1600445.

22. J.-N. Chazalviel, *Phys. Rev. A*, 1990, **42**, 7355.

23. C. Monroe and J. Newman, *J. Electrochem. Soc.*, 2005, **152**, A396-A404.

24. J. Zheng, M. H. Engelhard, D. Mei, S. Jiao, B. J. Polzin, J.-G. Zhang and W. Xu, *Nat. Energy*, 2017, **2**, 17012.

25. M. D. Tikekar, S. Choudhury, Z. Tu and L. A. Archer, *Nat. Energy*, 2016, **1**, 16114.

26. D. Zhou, R. Liu, Y. B. He, F. Li, M. Liu, B. Li, Q. H. Yang, Q. Cai and F. Kang, *Adv. Energy Mater.*, 2016, **6**, 1502214.

27. X. B. Cheng, R. Zhang, C. Z. Zhao, F. Wei, J. G. Zhang and Q. Zhang, *Adv. Sci.*, 2016, **3**, 1500213.

28. Z. Wan, D. Lei, W. Yang, C. Liu, K. Shi, X. Hao, L. Shen, W. Lv, B. Li and Q. H. Yang, *Adv. Funct. Mater.*, 2019, **29**, 1805301.

29. Q. Pan, D. M. Smith, H. Qi, S. Wang and C. Y. Li, *Adv. Mater.*, 2015, **27**, 5995-6001.

30. M. Chi, L. Shi, Z. Wang, J. Zhu, X. Mao, Y. Zhao, M. Zhang, L. Sun and S. Yuan, *Nano Energy*, 2016, **28**, 1-11.

31. Z. Tu, Y. Kambe, Y. Lu and L. A. Archer, *Adv. Energy Mater.*, 2014, **4**, 1300654.

32. C.-P. Yang, Y.-X. Yin, S.-F. Zhang, N.-W. Li and Y.-G. Guo, *Nat. Commun.*, 2015, **6**, 8058.

33. Q. Li, S. Zhu and Y. Lu, *Adv. Funct. Mater.*, 2017, **27**, 1606422.

34. H. Zhao, D. Lei, Y. B. He, Y. Yuan, Q. Yun, B. Ni, W. Lv, B. Li, Q. H. Yang and F. Kang, *Adv. Energy Mater.*, 2018, 1800266.

35. G. Zheng, S. W. Lee, Z. Liang, H.-W. Lee, K. Yan, H. Yao, H. Wang, W. Li, S. Chu and Y. Cui, *Nat. Nanotechnol.*, 2014, **9**, 618.

36. K. Liu, D. Zhuo, H. W. Lee, W. Liu, D. Lin, Y. Lu and Y. Cui, *Adv. Mater.*, 2017, **29**, 1603987.

37. W. Luo, L. Zhou, K. Fu, Z. Yang, J. Wan, M. Manno, Y. Yao, H. Zhu, B. Yang and L. Hu, *Nano Lett.*, 2015, **15**, 6149-6154.

38. M. E. Barbour, D. M. Parker and K. D. Jandt, *J. Colloid Interf. Sci.*, 2003, **265**, 9-14.

39. G. Dinda, J. Shin and J. Mazumder, *Acta Biomater.*, 2009, **5**, 1821-1830.

40. S. Habelitz, G. W. Marshall Jr, M. Balooch and S. J. Marshall, *J. Biomech.*, 2002, **35**, 995-998.

41. G. Stone, S. Mullin, A. Teran, D. Hallinan, A. Minor, A. Hexemer and N. Balsara, *J. Electrochem. Soc.*, 2012, **159**, A222-A227.

42. M. Wu, Z. Wen, Y. Liu, X. Wang and L. Huang, *J. Power Sources*, 2011, **196**, 8091-8097.

43. M. Tang, P. Albertus and J. Newman, *J. Electrochem. Soc.*, 2009, **156**, A390-A399.

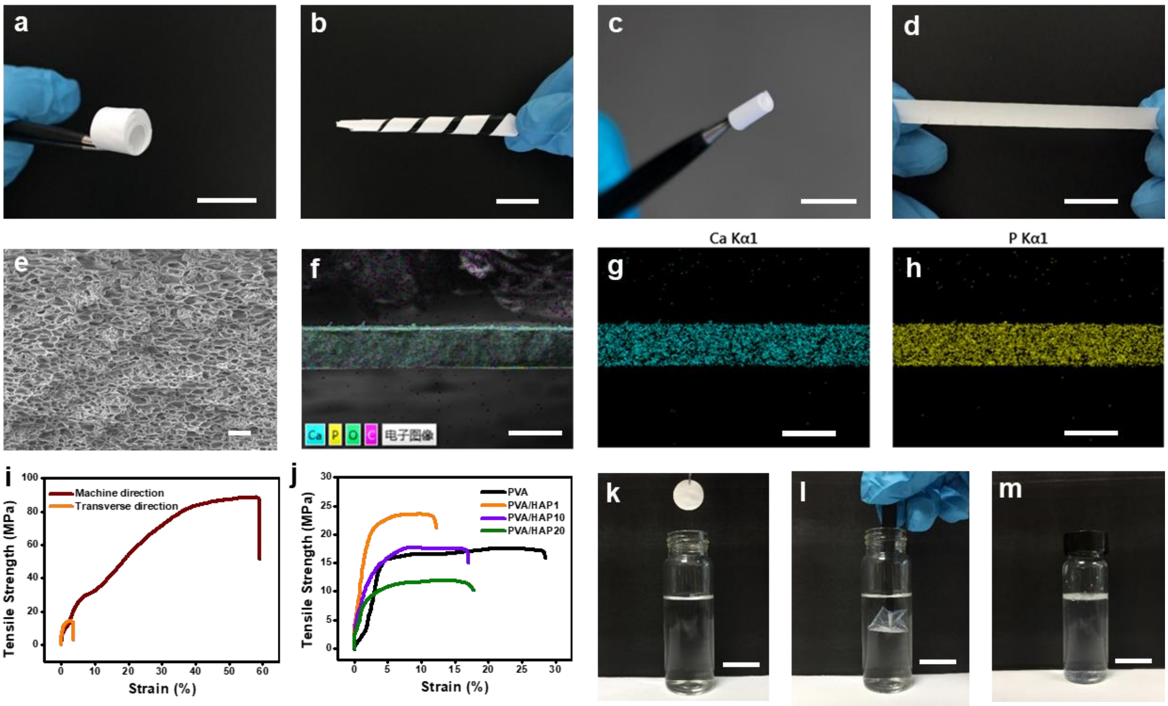

Figure 1. Flexibility, mechanical strength, microstructure and element mapping of the as-prepared 3D HAPs10%/PVA separator. High flexibility of the HAPs10%/PVA separator under different bending conditions: a) rolled, b) twisted, c) separator ribbon has been wound more than 10 times, and the radius thickness of the roll separator is nearly 0.5 mm, indicating its great rollability, d). After keeping the rolled state for 30 min, PVA/HAP10 separator was restored to its original state without any break. The white scale bar of above ribbons represents 2 cm. e) SEM image of cross-section of 3D HAPs10%/PVA membrane. The scale bar is 3 μm. f-h) SEM images of the cross-section with related element mapping of PVA/HAP10 separator. The white scale bar represents 50 um. Stress−strain curves of i) Celgard separator, and j) pristine PVA and HAPs/PVA separators, respectively. Digital photos of 3D HAPs10%/PVA with a diameter of 16 mm k) before and l) after immersing into the deionized water, m) after 20 s of shaking. The scale bar is 16 mm. The operation is conducted at room temperature (25 ℃).

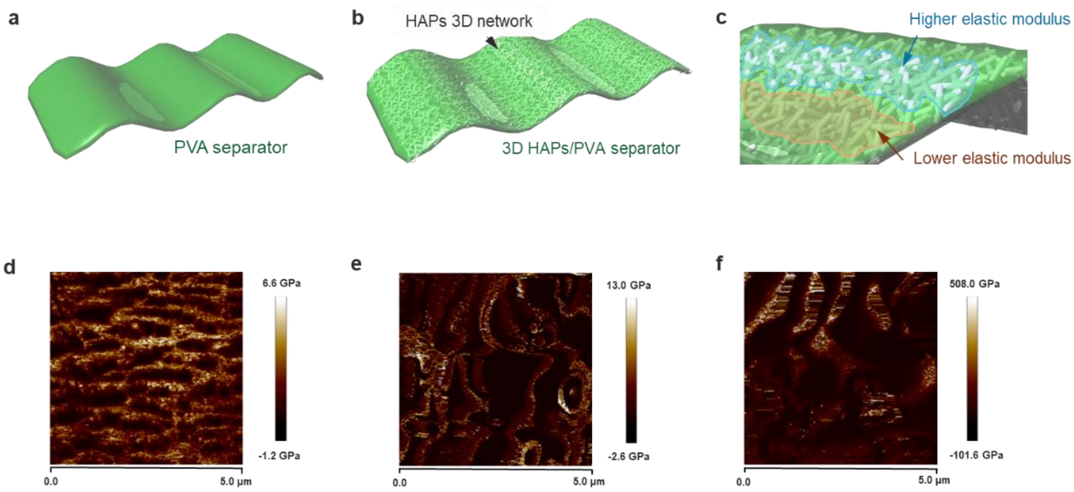

Figure 2. Schematic presentation of the separator design. a) Pristine PVA separator, b) 3D HAPs10%/PVA and c) magnification of 3D HAPs10%/PVA. The Young's modulus mapping of d) Celgard separator, e) pristine PVA separator and f) 3D HAPs10%/PVA separators.

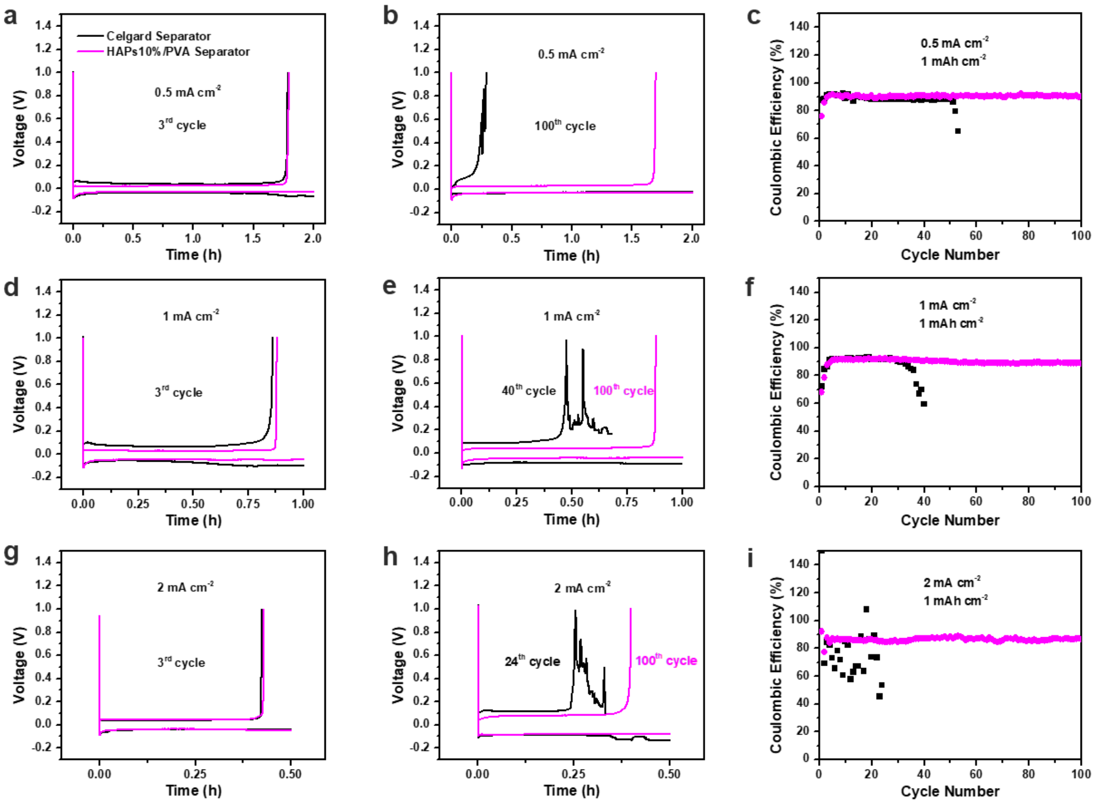

Figure 3. Electrochemical performance of Li|Cu cells with Celgard and 3D HAPs/PVA separators at different current densities with a lithiation capacity of 1.0 mAh cm^{-2}. Potential profiles for the third and dead cycle or 100th cycle at (a, b) 0.5 mA cm^{-2}, (d, e) 1.0 mA cm^{-2}, and (g, h) 2.0 mA cm^{-2}; Comparison of the Coulombic efficiency at (c) 0.5 mA cm^{-2}, (f) 1.0 mA cm^{-2}, and (i) 2.0 mA cm^{-2}.

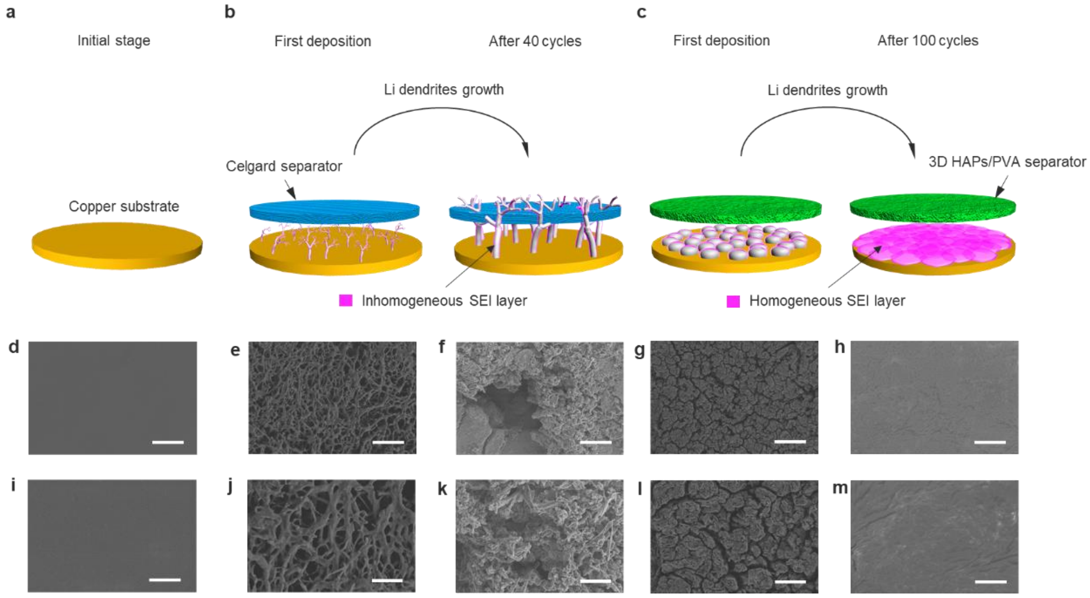

Figure 4. Schematic of the morphologies of Li deposited on the bare Cu substrate with different separators. Li dripping/stripping process are conducted at the current densities of 1 mA cm^{-2}, and the capacity for each Li deposition was set to be 1 mAh cm^{-2}. Schematic illustration showing a) the bare copper substrate and the growth process of dendritic Li on the surface of copper substrate with b) Celgard separator and c) 3D HAPs/PVA separator. SEM images of d, i) bare copper substrate, first Li deposition for e, j) Celgard separator and g, i) 3D HAPs/PVA separator, f, k) after 40 cycles for Celgard separator and h, m) after 100 cycles for 3D HAPs/PVA separator with the scale bar of 10 μm and 2 μm, respectively.

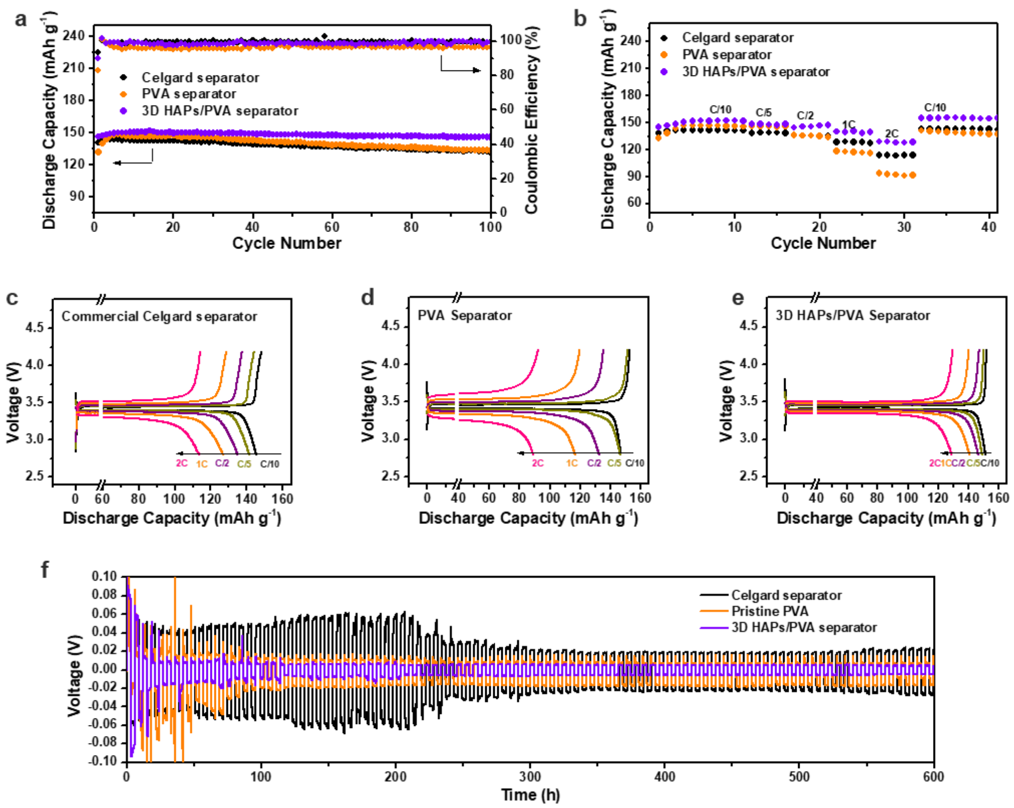

Figure 5. Cycling stability and rate performance of $LiFePO_4$|lithium metal batteries system employing different separators. a) Cycling performance of the cells with using the Celgard separator, pristine PVA separator, and the 3D HAPs/PVA separator at C/5 with a cutoff voltage of 2.8-4.2 V for 100 cycles. b) Rate performance of the cells using different separators with a cutoff voltage of 2.8-4.2 V. The first five cycles are run for the activation. Voltage profiles of the cells using c) the Celgard separator, d) control PVA separator and e) the 3D HAPs/PVA separator at C/10, C/5, C/2, C and 2C, respectively. f) The Li dripping/stripping of Li|separator-liquid electrolyte|Li symmetrical cells, which are charged and discharged for respective 3 h during each cycle, employing a constant current density of 0.5 mA cm^{-2}.